Materials Science in Semiconductor Processing 30 (2015) 85–91

Contents lists available at ScienceDirect

Materials Science in Semiconductor Processing

journal homepage: www.elsevier.com/locate/mssp

Deposition, opto-electronic and structural characterization of polymorphous silicon thin films to be applied in a solar cell structure

L. Hamui [a], A. Remolina [b], M.F. García-Sánchez [c], A. Ponce [d], M. Picquart [e], M. López-López [f], B.M. Monroy [a], G. Santana [a,f,*]

[a] Instituto de Investigaciones en Materiales, Universidad Nacional Autónoma de México. A.P. 70-360, Coyoacán, C.P. 04510 México, D.F., Mexico
[b] Grupo de Investigación en Desarrollo Tecnológico, Mecatrónica y Agroindustria (GIDETECHMA), Facultad de Ingeniería Mecánica, Universidad Pontificia Bolivariana de Bucaramanga. Km. 7 via a Piedecuesta, Floridablanca, Colombia
[c] Unidad Profesional Interdisciplinaria en Ingeniería y Tecnologías Avanzadas, Instituto Politécnico Nacional, Av. I.P.N. 2580, Gustavo A. Madero, 07340 México, D.F., Mexico
[d] Department of Physics and Astronomy, University of Texas at San Antonio, One UTSA Circle, San Antonio, TX 78249, USA
[e] Departamento de Física, Universidad Autónoma Metropolitana, AP 55-534, CP 09340 México, D.F., Mexico
[f] Departamento de Física, Centro de Investigación y Estudios Avanzados del IPN, CP 07360, México, D.F., Mexico

ARTICLE INFO

Available online 21 October 2014

Keywords:
Solar cells
PECVD
Polymorphous silicon
Thin films

ABSTRACT

In this study we analyze the optoelectronic properties and structural characterization of hydrogenated polymorphous silicon thin films as a function of the deposition parameters. The films were grown by plasma enhanced chemical vapor deposition (PECVD) using a gas mixture of argon (Ar), hydrogen (H_2) and dichlorosilane (SiH_2Cl_2). High-resolution transmission electron microscopy images and Raman measurements confirmed the existence of very different internal structures (crystalline fractions from 12% to 54%) depending on the growth parameters. Variations of as much as one order of magnitude were observed in both the photoconductivity and effective absorption coefficient between the samples deposited with different dichlorosilane/hydrogen flow rate ratios. The optical and transport properties of these films depend strongly on their structural characteristics, in particular the average size and densities of silicon nanocrystals embedded in the amorphous silicon matrix. From these results we propose an intrinsic polymorphous silicon bandgap grading thin film to be applied in a p–i–n junction solar cell structure. The different parts of the solar cell structure were proposed based on the experimental optoelectronic properties of the pm-Si:H thin films studied in this work.

© 2014 Elsevier Ltd. All rights reserved.

1. Introduction

Hydrogenated polymorphous silicon (pm-Si:H) as a new material for solar cells has been the subject of scientific and technological interest in recent years because of its outstanding properties such as higher electrical conductivity, greater doping efficiency [1–3], lower defect densities, low fabrication cost and scalable process. The expectation is that replacing hydrogenated amorphous silicon (a-Si:H) by different forms of

* Corresponding author at: Instituto de Investigaciones en Materiales, Universidad Nacional Autónoma de México. A.P. 70-360, Coyoacán, C.P. 04510 México, D.F., Mexico.
Tel.: +52 55 56224577; fax: +52 55 56161251.
E-mail addresses: lhamui@iim.unam.mx (L. Hamui), aduljayr@yahoo.com (A. Remolina), rusonil@yahoo.com (M.F. García-Sánchez), arturo.ponce@utsa.edu (A. Ponce), mp@xanum.uam.mx (M. Picquart), mlopez@fis.cinvestav.mx (M. López-López), marel@iim.unam.mx (B.M. Monroy), gsantana@iim.unam.mx (G. Santana).

http://dx.doi.org/10.1016/j.mssp.2014.09.042
1369-8001/© 2014 Elsevier Ltd. All rights reserved.

pm-Si:H thin films can reduce the cost of "solar electric power" by increasing the efficiency and stability of silicon-based thin film photovoltaic devices [4]. Hydrogenated polymorphous silicon consists of small silicon nanocrystals (~2–10 nm) embedded in an amorphous silicon matrix. These are formed near dusty plasma conditions in order to obtain the crystallites within the plasma and to obtain high deposition rates with small to medium crystalline fractions [2,3]. The optical bandgap of hydrogenated polymorphous silicon thin films can be varied by varying the size distribution and the density of the nanocrystals, which can be easily tailored by controlling the deposition parameters [2,3,5,6]. Indeed the optical properties, such as the absorption coefficient, depend mainly on the amorphous matrix while the transport properties, such as the conductivity, are related to the crystallites' size and density.

Polymorphous silicon based thin-film single junction solar cells have a p–i–n or n–i–p structure depending on the deposition sequence of doped and intrinsic layers. For both structures the light enters through the p-layer which efficiently supports hole collection in the device, since the mobility of holes is smaller compared to the mobility of electrons. The p–i–n deposition sequence requires that pm-Si:H is deposited onto a transparent substrate that typically consists of a low-cost glass covered with a transparent conductive oxide (TCO). The back contact is generally a highly reflecting metal layer, possibly deposited onto a refractive index matching interlayer. The majority of manufacturers use this p–i–n approach, often called a superstrate configuration [8].

Each of the individual layers that compose the cell must have particular characteristics. A very thin (10–30 nm) p^+-layer with a wide bandgap (2–2.3 eV) of a-Si:H can be applied as window layer to reduce absorption losses. A sufficiently high electrical conductivity is needed in the p-layer to guarantee a low series resistance as well as a high open-circuit voltage. For the intrinsic i-layer (300–500 nm) it is desirable to have pm-Si:H with higher absorption coefficient and optimal bandgap (1.6–1.8 eV). This material must have a high photoconductivity and thus guarantee a high mobility of carriers. The n^+-layer (20–30 nm) must have similar electrical properties to those of the p^+-layer to build up an intense internal electric field. The optical bandgap of this layer has to be the smallest in the structure (1.5–1.6 eV) to absorb the remaining low energy solar radiation.

In this work pm-Si:H thin films with different internal structures were deposited, varying the growth parameters. Absorption and photoconductivity properties were analyzed as a function of the microstructural characteristics of the films. We propose an intrinsic polymorphous silicon bandgap grading thin film to be applied in a p–i–n junction solar cell structure. The solar cell structure was designed based on the experimental optoelectronic properties of the pm-Si:H thin films.

2. Experimental

Hydrogenated polymorphous silicon films were deposited on quartz substrates by plasma enhanced chemical vapor deposition (PECVD), using a 13.56 MHz discharge of (99.9999% purity) $SiH_2Cl_2+H_2+Ar$. A conventional PECVD system with parallel plates of 127 cm^2 surface and 1.5 cm apart was used. Prior to deposition, the chamber of the PECVD system was evacuated to a pressure of 10^{-6} Torr. Further details of the deposition process can be found elsewhere [7,9]. The process parameters such as the chamber pressure (250 mTorr), the substrate temperature (200 °C), and Ar flow rate (50 sccm) were maintained constant while the dichlorosilane/hydrogen flow rate ratio and applied RF power were varied. The structural properties of the pm-Si:H films were modified by changing the flow rate ratio and RF power in the reaction chamber. The flow rate ratio is defined by $R=[SiH_2Cl_2]/[H_2]$ and varied from 0.05 to 0.1 changing the flow rate of dichlorosilane from 2.5 to 5 sccm while hydrogen flow rate is maintained constant (50 sccm), and RF power is varied with the following values: 10, 25, 50, 100 and 150 W.

The deposited films were analyzed by Raman scattering and high resolution transmission electron microscopy (HRTEM) for structural characterization. The Raman spectra were recorded using a T64000 Jobin-Yvon Horiba triple monochromator using as excitation source the 514.5 nm line from an Ar+Lexcel laser. All the measurements were performed at room temperature in open air and acquired by a cooled CCD detector. A spot size of 3.14 mm^2 and an irradiation power of 20 mW were selected in order to avoid any beam-induced structural changes during measurements. The measuring range and integration time were 400–600 cm^{-1} and 1 min, respectively. HRTEM studies were conducted in a FEI-Titan 80–300 kV microscope. The images were obtained in the Scherzer focus and recorded simultaneously online with a CCD camera. The Gatan DigitalMicrograph™ software was used for analysis of HRTEM images. The samples thickness was measured using a Veeco Dektak 150 profilometer with a vertical resolution of 5 nm. Transmission measurements were recorded in a UV–vis spectrometer Jasco V-630 in a two-beam configuration. The measurement range selected for the transmission spectra was between 200 and 1100 nm. Transmission spectra were used to determine the effective absorption coefficient (α_{eff}). It is called effective because it does not consider the reflected and dispersed photons; since it is calculated as $\alpha_{eff}=[\ln(100/T)]/d$ where T is the percentage of transmitted photons and d is the film thickness in cm. Dark conductivity (σ_D) and illuminated conductivity (σ_I) were measured using a Keithley 617 programmable electrometer on planar geometry using a halogen lamp with an intensity of 100 mW/cm^2 and with a similar spectrum to the solar spectrum. Photoconductivity was calculated as $\Delta\sigma=\sigma_I-\sigma_D$ and the photosensitivity as $\Delta\sigma/\sigma_D$. Silver electrodes were evaporated on the pm-Si:H films in vacuum lower than 10^{-5} Torr for electrical measurements.

3. Results and discussion

HRTEM images in Fig. 1 show the average size and density of nanocrystallites for films grown with different R and RF powers. Fig. 1a and c shows that at lower RF powers (50 W) the matrix is predominantly amorphous with small crystallites. The increase in RF power increases the density of nanocrystallites in the film (Fig. 1b and d).

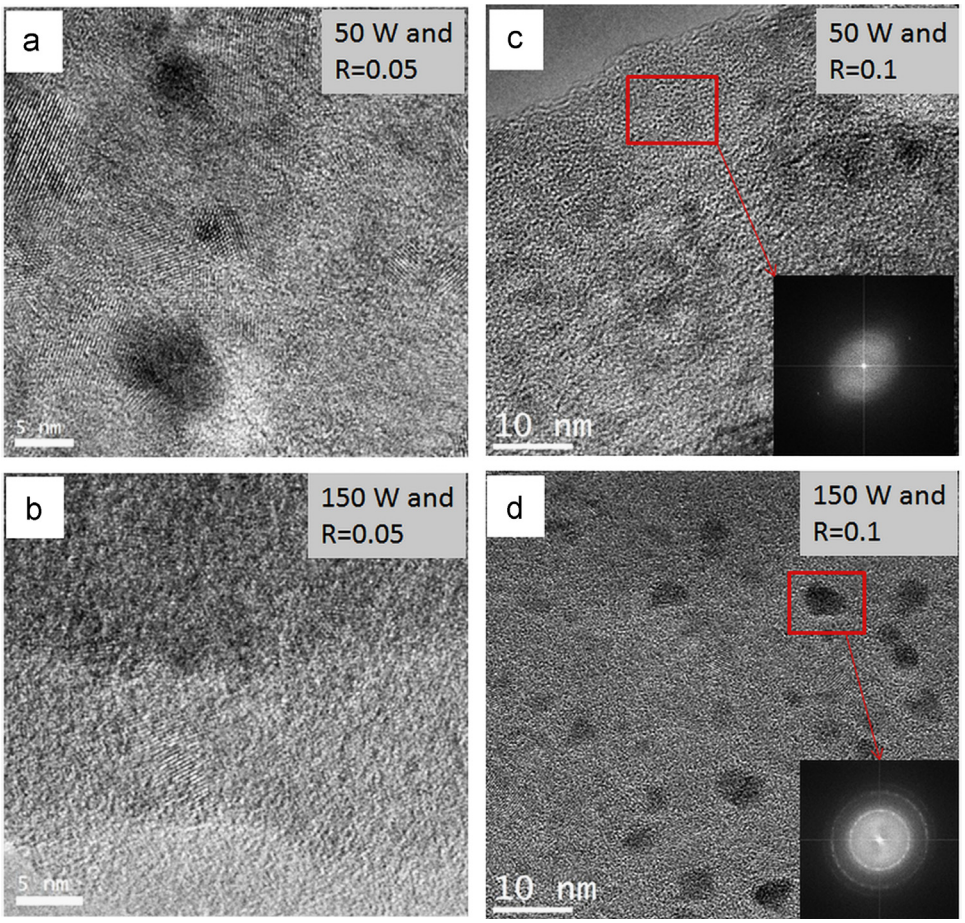

Fig. 1. HRTEM images from pm-Si:H films grown with (a) 50 W and $R=0.05$, (b) 50 W and $R=0.1$, (c) 150 W and $R=0.05$, and (d) 150 W and $R=0.1$. Also diffraction patterns for the samples with 50 W and 150 W for the $R=0.1$ series are shown as insets.

On the other hand, decreasing R increases the size and density of crystallites for the same RF power. This change in the crystallinity is more pronounced for higher RF power (Fig. 1a and b). These HRTEM images evidence that by regulating the RF power and dichlorosilane/hydrogen ratio, polymorphous silicon thin films with very different microstructures can be obtained: from predominantly amorphous with small nanocrystallites (Fig. 1c) to almost nanocrystalline (Fig. 1b). A diffraction pattern inset is shown in Fig. 1c and d in order to show the variation of the crystalline phase in the films with the deposition parameters. For the first one, randomly and dispersed dots can be seen indicating a mostly amorphous phase in the analyzed zone. However, for the sample deposited with higher power, diffraction rings related to different crystalline orientations are observed supporting the previous observations. Fig. 2a shows a HRTEM image for the sample grown with 150 W and $R=0.1$ showing the amorphous and crystalline phases clearly. The latter supports the definition of hydrogenated polymorphous silicon in our materials and also evidences the presence of the small nanocrystals. In Fig. 2b the variation of the nanocrystals sizes as a function of the deposition RF power for $R=0.1$ is shown. As can be appreciated the average nanocrystals sizes are between 2.5 and 12 nm, which is in accordance with the hydrogenated polymorphous silicon definition. Furthermore, there is a slight increase of the average sizes with RF power and then a decrease to 7 nm for the sample deposited with 150 W. Table 1 shows the variation of the film thickness with the deposition parameters. It can be seen that there is no direct relation with the increasing power for $R=0.1$ but for $R=0.05$ it appears to have an increasing trend with power except for the sample of 100 W. Also we can identify that there is a minimum for $R=0.05$ and 100 W and a maximum for $R=0.1$ and 150 W in the film thickness.

We performed Raman spectroscopy in order to describe quantitatively the variations of the crystallite volume fraction (X_C) of the films. Fig. 3 shows representative Raman spectra of films deposited with different flow rate ratios R and different RF powers. In general, for amorphous/crystalline mixed phase silicon thin films such as pm-Si:H, we consider that the Raman spectrum consists of three contributions to the transverse optical (TO) mode peak: a sharp peak around 520 cm^{-1}, an intermediate peak between 500 and 519 cm^{-1} and a broad peak around 480 cm^{-1} which correspond to the crystalline, grain boundaries and nanocrystalline, and amorphous phases, respectively [10]. For 50 W we can observe

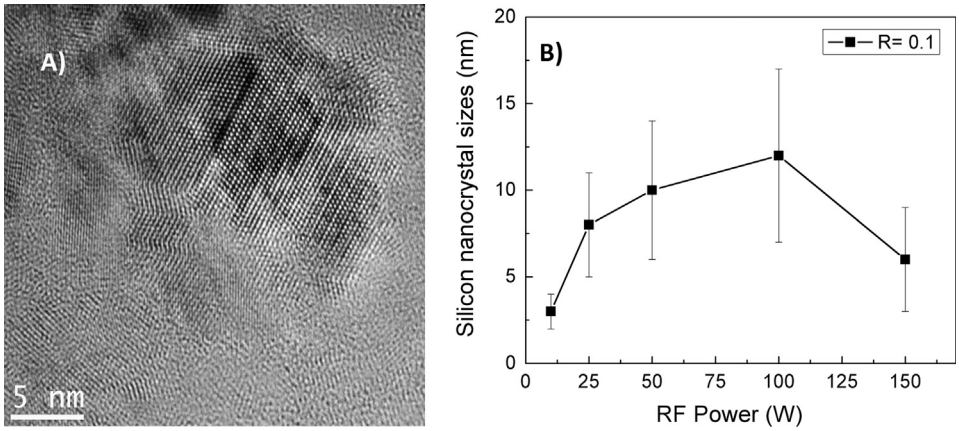

Fig. 2. (a) HRTEM image from pm-Si:H films grown with 150 W and $R=0.1$ showing the amorphous and crystalline phases and (b) the silicon average nanocrystals size for $R=0.1$ as a function of RF power.

Table 1
Crystalline fraction, thickness and optical gap energies for the different deposition parameters.

R	Power (W)	Crystalline fraction (%)	Thickness (nm)	Eg (eV)
0.1	10	18 ± 0.73	370 ± 5	1.74 ± 0.02
	25	19 ± 0.78	325 ± 5	1.77 ± 0.02
	50	22 ± 0.90	250 ± 5	2.20 ± 0.02
	100	22 ± 0.89	305 ± 5	1.88 ± 0.02
	150	27 ± 1.11	550 ± 5	2.09 ± 0.02
0.05	10	13 ± 0.53	135 ± 5	1.65 ± 0.02
	25	27 ± 1.10	155 ± 5	2.03 ± 0.02
	50	25 ± 1.02	170 ± 5	1.92 ± 0.02
	100	12 ± 0.50	110 ± 5	1.82 ± 0.02
	150	54 ± 2.19	180 ± 5	1.86 ± 0.02

that the samples are predominantly amorphous since the Raman signal consists of a broad peak centered around 480 cm^{-1}. With the increase of the RF power a sharper peak centered close to 520 cm^{-1} is observed, indicating that the films are more crystalline with respect to the samples deposited at 50 W. However, at lower R the crystallinity is increased with increase in RF power (Fig. 3a). For the sample deposited with 150 W and $R=0.05$ a very sharp peak centered around 507 cm^{-1} evidences the nanocrystalline structure of the sample, while for the sample deposited at 50 W a shoulder around 510 cm^{-1} can be distinguished which suggests a nanocrystalline contribution to the spectrum. All these results confirm the trends observed by HRTEM and agree with the pm-Si:H definition.

The Raman spectra of the samples were analyzed by deconvolution into 3 Gaussian peaks corresponding to the crystalline (520 cm^{-1}), nanocrystalline (500–519 cm^{-1}) and amorphous (480 cm^{-1}) phase and the areas of each peak were used to calculate the crystalline fraction (X_C). This parameter can be calculated by the expression $X_C = I_C/(I_C+yI_a)$ [11], where I_C is the sum of the areas corresponding to the nanocrystalline and crystalline TO Peaks, I_a is the area corresponding to the amorphous TO peak and y is the absorption cross section ratio which has a value $y \cong 0.99$, so we used $y=1$ for our samples [12]. Important changes in the crystalline fraction, from 12% to 54%, were obtained with the variation of R and the RF power as shown in Table 1. For $R=0.1$ the crystalline fraction increases with the increase of RF power. The increase of the crystalline fraction with RF power comes along with an increase of the nanocrystals sizes as observed in Fig. 2b, except for the sample deposited at 150 W where the size is reduced, indicating that the density of the nanocrystals must have increased. However, for $R=0.05$ the crystalline fraction has an anomalous behavior with the increase of RF power. In this case as the power increases from 10 W to 25 W the crystalline fraction increases and for powers of 50 W and 100 W, it decreases again. At 100 W it shows the lowest crystallinity, while at 150 W it shows the highest crystallinity and the highest value for both flow rate ratios. As observed in Table 1 there is a variation of the film thickness along with the deposition parameters (R and RF power). We believe that there are changes in the plasma–surface interactions which could represent the main factors for the induced crystallinity during growth. This can be related to a combination of growth and etching regimes with higher amounts of hydrogen in the plasma during deposition [13]. Moreover, since we use dichlorosilane as precursor gas, chlorine chemistry is affected by changes in R and RF power and this affects the behavior of the crystalline fraction in the PECVD process. In the SiH_2Cl_2 system, when SiH_xCl_y $(x+y<3)$ radicals arrive at the growing surface, both hydrogen and chlorine are preferentially extracted as HCl and bring forth the film deposition. Incrementing hydrogen dilution (lower R, in this case) promotes interactions between atomic H and Si–H and Si–Cl bonds that result in higher density of nucleation sites and increased chlorine extraction from the film, but also an enhancement of ion bombardment and attack of the growing surface [10]. Chlorine extraction from the surface involves exothermic reactions with atomic hydrogen which releases a considerable amount of energy that induces local crystallization [14]. Thus, there are two competing phenomena involved: ion bombardment and local crystallization that can explain the anomalous trend in X_C observed for lower R and also explain the variation of the surface thickness during growth.

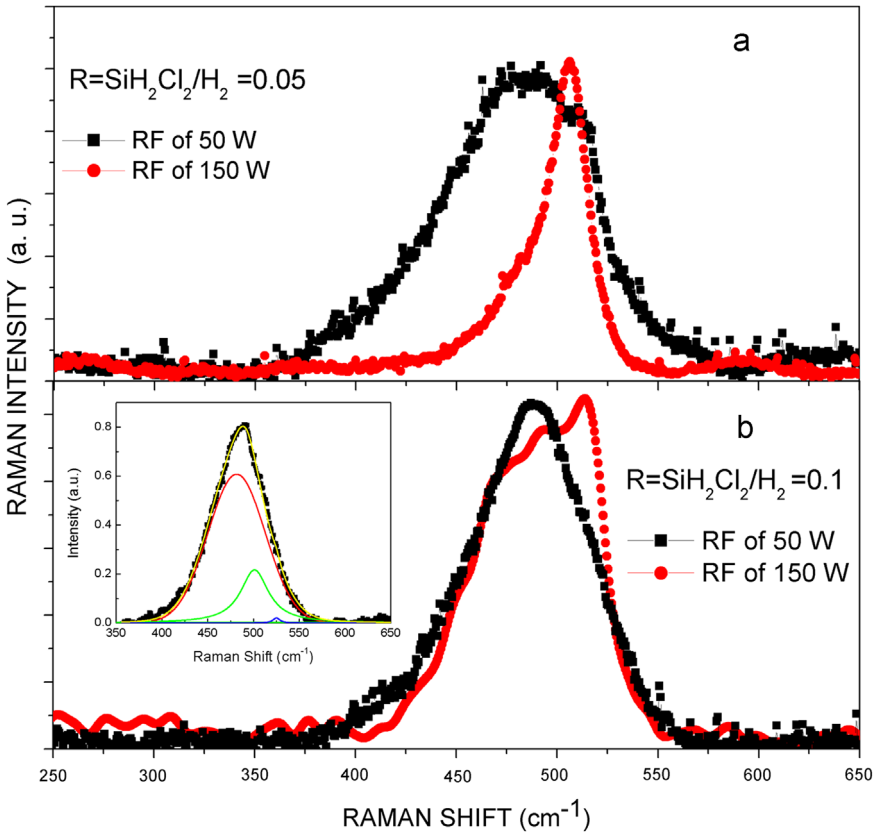

Fig. 3. Raman spectra from pm-Si:H films grown with (a) $R=0.05$ and (b) $R=0.1$ and different RF powers. A Raman spectra deconvolution for $R=0.1$ and 50 W is shown as an inset.

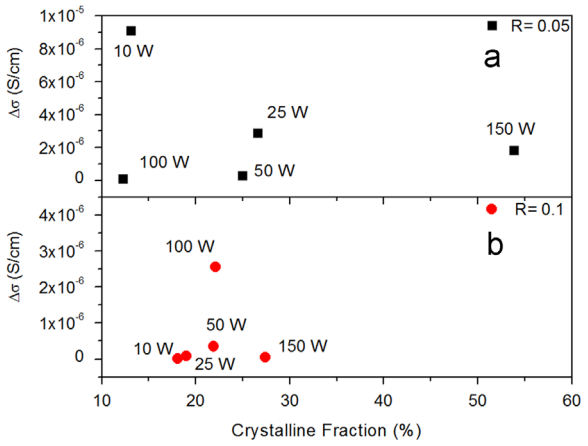

Fig. 4. Photoconductivity vs. crystalline fraction of pm-Si:H films grown with (a) $R=0.05$ and (b) $R=0.1$ with different RF powers.

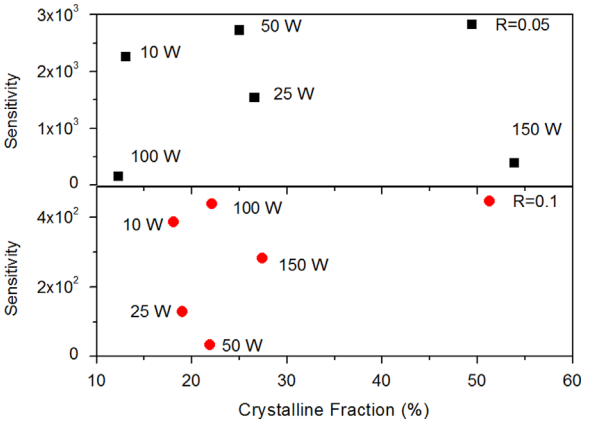

Fig. 5. Photosensitivity vs. crystalline fraction of pm-Si:H films grown with (a) $R=0.05$ and (b) $R=0.1$ with different RF powers.

The photoconductivity of the films deposited with different R and RF powers are shown in Fig. 4. For the samples deposited with lower R, important changes in the photoconductivity are appreciated (Fig. 4a). It is worth noting that there can be as much as one order of magnitude difference between the photoconductivity of the sample deposited at 10 W and the sample deposited at 150 W. There is no explicit trend of the photoconductivity as a function of only the crystalline fraction in the films. The transport properties in this material are also influenced by the structural disorder caused by crystallite size variations, grain boundaries, amorphous phase and voids [15]. An increase of atomic hydrogen bombardment from the plasma may cause ion-induced desorption of hydrogen from the surface during growth [13]. This process affects considerably the optoelectronic properties of the amorphous matrix since the removal of bonded hydrogen can lead to dangling bonds and increase of the structural disorder. This

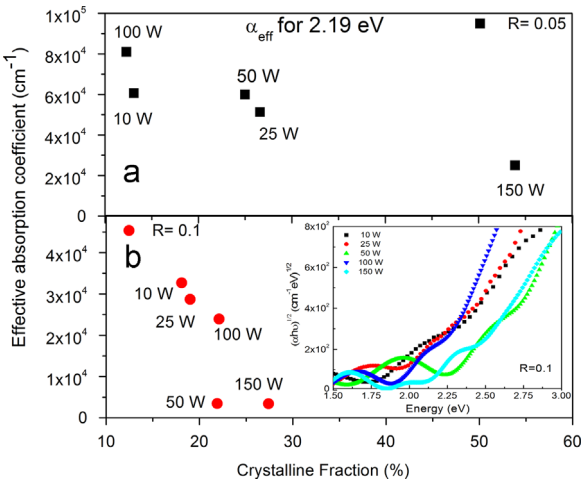

Fig. 6. Effective absorption coefficient at 2.19 eV from pm-Si:H films grown with (a) $R=0.05$ and (b) $R=0.1$ with different RF powers. A representative Tauc-plot for $R=0.1$ is shown as an inset.

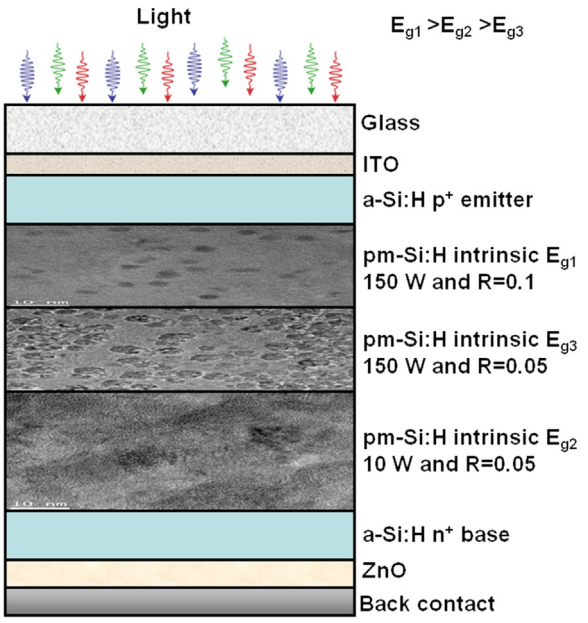

Fig. 7. Schematic representation of an intrinsic polymorphous silicon bandgap grading thin film applied in a p–i–n solar cell structure.

effect is diminished by increasing R. In Fig. 4b, we can observe that the photoconductivity has a smaller variation as a function of the crystalline fraction compared to the samples deposited at $R=0.05$. Fig. 5 shows the photosensitivity as a function of the crystalline fraction. It is observed that pm-Si:H films present a high photoresponse with sensitivity values up to 2.8×10^3. For lower R the photosensitivity has a variation of up to one order in magnitude between samples, whereas for higher R it shows a slight variation with the crystalline fraction. This result is expected since the highest structural variation in the samples is observed for $R=0.05$. For $R=0.1$ it is observed that the photosensitivity between samples varies very slightly; moreover, it is one order of magnitude lower than for most of the samples grown with $R=0.05$. This confirms that the variation in the electronic properties cannot be described as only a function of the crystalline fraction.

To compare the absorption properties of the films an effective absorption coefficient (α_{eff}) was calculated at fixed photon energy of 2.19 eV which is in the region of maximum intensity of the solar spectrum. Fig. 6 shows the effective absorption coefficient of the pm-Si:H films as a function of crystalline fraction. The absorption coefficient decreases as the crystalline fraction increases for both R values. The value of α at 2.19 eV for standard a-Si:H is $8\times10^4\ cm^{-1}$ and for crystalline silicon is $8\times10^3\ cm^{-1}$ [16]. In Fig. 6 we can appreciate that for both R ratios the effective absorption coefficient shows a decreasing trend with the crystalline fraction. We can observe from Fig. 6 that the α_{eff} of some of the samples deposited at low R is close to the absorption values of a-Si:H, while the samples deposited at higher R have absorption properties more similar to those of crystalline silicon. These results show that we can obtain very different absorption properties in pm-Si:H depending on the growth parameters and furthermore they can be tailored by varying the nanocrystals size and density in accordance with the pm-Si:H definition. Finally, the optical gap values were calculated using the Tauc model from the UV–vis measurements. These results are presented in Table 1 and in Fig. 6 a representative Tauc-plot for $R=0.1$ is shown as an inset. The measurement range shown for the Tauc-plot is between 410 and 820 nm which is the range of interest for photovoltaic materials with optical gaps between 1.1 and 2.2 eV, as in the materials studied in this work. It is observed that the optical gap values for both flow rate ratios are between 1.65 eV and 2.2 eV. As in the case of the transport properties, there is no clear trend with the crystalline fraction. Other effects, such as quantum confinement in nanocrystals, should be taken into account to explain the tendency in the optical gaps, as well.

An intrinsic polymorphous silicon bandgap grading thin film was proposed to be applied in a p–i–n solar cell structure according to the optical and transport properties of the pm-Si:H films discussed previously. A schematic representation of this structure is presented in Fig. 7. The intrinsic film is located between a-Si:H p-type and n-type layers in order to generate an electric field separating the electron–hole pairs and driving each to the corresponding contacts. Further details of these materials can be found elsewhere [4]. The device is illuminated through the glass and photons cross the TCO layer and the emitter to reach the intrinsic pm-Si:H layer to be absorbed. A ZnO buffer layer was selected to lower the potential contact between the back contact and the base layer. The film with higher bandgap was the one deposited at 150 W and $R=0.1$ (Table 1), so we selected it as the top layer beneath the emitter because absorption of high energy photons is desirable at the top of the structure. On the other hand, for the middle layer we chose the film deposited at 150 W and $R=0.05$ which presents the highest crystalline fraction and a smaller bandgap than those of the previous layer. Finally, for the main absorber we selected the film deposited at 10 W and $R=0.05$ as the back layer because it presents the highest photoconductivity, absorption properties and the lowest bandgap. This design improves the absorption

properties of conventional p–i–n structures and should increase the conversion efficiency of the solar cell devices. This is due to the photon absorption range control as a consequence of an optimal crystalline fraction selection and the related properties within the different intrinsic pm-Si:H layers which generates a better carrier collection probability, increasing the internal quantum efficiency of a solar cell. An advantage of this proposed structure is that it consists of the same type of silicon alloy and the different layers can be easily achieved by variation of the deposition parameters in the same deposition process.

4. Conclusions

Varying the dichlorosilane/hydrogen flow rate ratio and RF power during the PECVD process we obtained pm-Si:H thin films with very different internal structures. The optical and transport properties of these films depend strongly on their structural characteristics. The crystalline fraction is not enough as a parameter to describe the change of electronic properties in pm-Si:H thin films; other structural information such as the size and density of the nanocrystalline inclusions should be taken into account too. Variations of as much as one order of magnitude were observed in both the photoconductivity and effective absorption coefficient of the samples deposited with different *R*. These results allowed the design of an intrinsic polymorphous silicon bandgap grading thin film applied in a p–i–n solar cell structure. The solar cell structure was proposed based on the experimental optoelectronic properties of the pm-Si:H thin films. An advantage of this type of structure is that it consists of the same type of silicon alloy and the different layers can be easily achieved by variation of the deposition parameters in the same deposition process.

Acknowledgments

We acknowledge partial financial support for this work from DGAPA-UNAM PAPIIT Projects IB101612 and IN100914, CONACYT, Mexico, under Projects 153948 and 179632, and SENER-CONACYT Project 151076. The authors are grateful to Dr. J.C. Alonso and Dr. A. Ortiz† for the use of laboratory facilities for samples preparation. A special acknowledgment is due to financial support from Consejo Nacional de Ciencia y Tecnología (CONACYT) through doctoral scholarship CVU 297213. Partial support from Instituto Politécnico Nacional (IPN), Mexico, with research project 20130293 is gratefully acknowledged. Thanks are also due to J. Camacho, C. González and O. Jiménez for technical and information support.

Appendix A. Supporting information

Supplementary data associated with this article can be found in the online version at http://dx.doi.org/10.1016/j.mssp.2014.09.042.

References

[1] R. Saleh, N.H. Nickel, Thin Solid Films 427 (2003) 266–269.
[2] P. Roca i Cabarrocas, A. Fontcuberta, S. Lebib, Y. Poissant, Pure Appl. Chem. 74 (3) (2002) 359–367.
[3] P. Roca i Cabarrocas, J. Non-Cryst. Solids 266–269 (31–37) (2000) 5453–5458.
[4] K.H. Kim, E.V. Johnson, P. Roca i Cabarrocas, Sol. Energy Mater. Sol. Cells 105 (2012) 208–212.
[5] J. Kitao, H. Harada, N. Yoshida, Y. Kasuya, M. Nishio, T. Sakamoto, T. Itoh, S. Nonomura, S. Nitta, Sol. Energy. Mater. Sol. Cells 66 (2001) 245–251.
[6] J. Meier, R. Fluckiger, H. Keppner, A. Shah, Appl. Phys. Lett. 65 (1994) 860–862.
[7] A. Remolina, B.M. Monroy, M.F. García-Sánchez, A. Ponce, M. Bizarro, J.C. Alonso, A. Ortiz, G. Santana, Nanotechnology 20 (2009) 245604.
[8] A. Kolodziej, C.R. Wronski, P. Krewniak, S. Nowak, Opto-electron. Rev. 8 (2000) 339.
[9] A. Remolina, L. Hamui, B.M. Monroy, M.F. García-Sánchez, A. Ponce, M. Picquart, G. Santana, Phys. Status Solidi C 8 (2011) 850–853.
[10] C. Álvarez-Macías, B.M. Monroy, L. Huerta, M.A. Canseco-Martínez, M. Picquart, J. Santoyo-Salazar, M.F. García-Sánchez, G. Santana, Appl. Surf. Sci. 285P (2013) 431–439.
[11] E. Bustarret, M.A. Hachicha, M. Brunel, Appl. Phys. Lett. 52 (1988) 1675–1677.
[12] A. Gajović, D. Gracin, K. Juraić, J. Sancho-Parramon, M. Čeh, Thin Solid Films 517 (18) (2009) 5453–5458.
[13] E.A.G. Hamers, A. Fontcuberta i Morral, C. Niikura, R. Brenot, P. Roca i Cabarrocas, J. Appl. Phys. 88 (2000) 3674–3688.
[14] B.M. Monroy, G. Santana, A. Benami, A. Ortiz, J.C. Alonso, J. Fandiño, F. Cruz-Gandarilla, J. Aguilar-Hernández, G. Contreras-Puente, A. López-Suárez, A. Oliver, J. Nanosci. Nanotechnol. 9 (2009) 2902–2909.
[15] K. Lips, P. Kanschat, W. Fuhs, Sol. Energy Mater. Sol. Cells 78 (2003) 513–541.
[16] M.A. Green, M.J. Keevers, Prog. Photovolt.: Res. Appl. 3 (1995) 189–192.